Iron−Cobalt Alloy Nanoparticles Embedded in an Alumina Xerogel Matrix

Guido Ennas,* Andrea Falqui, Giorgio Paschina, and Giaime Marongiu

Dipartimento di Scienze Chimiche, Università di Cagliari, S.S.554 Bivio per Sestu, 09042 Monserrato (Cagliari), Italy

Received August 3, 2005. Revised Manuscript Received September 21, 2005

Nanocrystalline γ-Al_2O_3 and FeCo−Al_2O_3 nanocomposite xerogels with high surface areas and pore volumes were prepared from alcogels obtained by a fast sol−gel procedure. The formation of γ-Al_2O_3 occurs via a sequence of stages starting from a disordered pseudo-bohemite phase which around 700 °C gives rise to amorphous allumina; this progressively cristallizes as γ-Al_2O_3, which is stable up to 1100 °C, when microcrystalline α-Al_2O_3 becomes the dominant phase; in the range 1000−1200 °C minor traces of δ-Al_2O_3 and θ-Al_2O_3 are present. Xerogels containing iron and cobalt are amorphous up to 700 °C; calcination at 800 °C gives rise to a spinel phase similar to γ-Al_2O_3 where metal ions partially fill the vacancies; at 1000 °C γ-Al_2O_3 progressively disappears to form α-Al_2O_3 and Co(Fe)Al_2O_4, which are the only phases present at 1200 °C. Reduction in hydrogen flow of the xerogel, previously calcined at 450 °C, leads to a nanocomposite constituted of FeCo alloy nanoparticles around 10 nm dispersed into α-Al_2O_3 nanocrystalline matrix. Zero-field-cooled (ZFC) and FC magnetic curves are typical of superparamagnetic materials and indicate the occurrence of high-strength particle interactions.

Introduction

Nanocomposite materials constituted by metal or alloy nanoparticles dispersed in crystalline or amorphous matrixes are of great interest because they combine individual properties of the constituent phases giving rise to new functional materials.[1,2] Among the preparation methods developed for their synthesis sol−gel allows the low-temperature preparation of well-dispersed nanoparticles in a matrix which tends to exhibit mesoporous structural features, giving the composites high porosities. As such they are largely employed as heterogeneous catalysts and chemical sensors;[3−5] moreover, the highly dispersed embedded particles facilitate investigations of magnetic properties, since interparticle interactions can be minimized.[6]

FeCo−SiO_2 nanocomposites constituted of FeCo alloy nanoparticles dispersed into amorphous silica were recently obtained in our laboratories in the form of xerogel, aerogel, and films.[7−10] These materials were prepared by simultaneous hydrolysis and condensation of either cobalt and iron nitrates or acetates with silicon tetrahydroxysilane (TEOS). The samples were shown to be very easily reducible, giving rise to FeCo nanocrystalline particles with the desired composition highly dispersed in the matrix.

Since the matrix is expected to influence the formation and growth of the dispersed nanoparticles, but also the resulting magnetic properties of the nanocomposite xerogels, it was considered interesting to investigate the possibility of obtaining the FeCo alloy nanoparticles within a different matrix, such as Al_2O_3.

In this work, FeCo−Al_2O_3 nanocomposite xerogels were studied together with pure alumina xerogels, which were prepared as a reference material. The samples submitted to thermal treatments both in oxidizing and reducing conditions were characterized by thermogravimetric analysis (TG), differential thermal analysis (DTA), N_2-physisorption at 77K, X-ray diffraction (XRD), and transmission electron microscopy (TEM). Measurements of magnetization as a function of temperature were performed on the reduced samples by superconducting quantum interference device (SQUID) magnetometer.

Experimental Section

Al_2O_3 alcogel was prepared by a procedure similar to the one described in ref 11: aluminum tri-*sec*-butoxide ($Al(OC_4H_9^{sec})_3$, Aldrich 97%, ASB) was dissolved in ethanol (Carlo Erba 99.8%, EtOH) at 80 °C and partially hydrolyzed with water diluted in ethanol containing nitric acid, to keep the pH of this hydrolyzing

* To whom correspondence should be addressed. Phone: +39 070 6754364. Fax: +39 070 6754388. E-mail: ennas@unica.it.

(1) Singh Nalwa, H., Ed. *Handbook of Nanostructured Materials and Nanotechnology*; Academic Press: San Diego, 2000.
(2) Klabunde, K. J. *Nanoscale Materials in Chemistry*; Wiley-Interscience: New York, 2001.
(3) Claus, P.; Brueckner, A.; More, C.; Hofmeister, H. *J. Am. Chem. Soc.* **2000**, *122*, 11430.
(4) Nagaraju, N.; Fonseca, A.; Konya, Z.; Nagy, J. B. *J. Mol. Catal. A: Chemical* **2002**, *181*, 57.
(5) Bharathi, S.; Nogami, M. *Analyst* **2001**, *126*, 1919.
(6) MacLaren, J. M.; Schulthness, T. C.; Butler, B. H.; Sutton, R.; McHenry, M. *J. Appl. Phys.* **1999**, *85*, 4833.
(7) Casula, M. F.; Corrias, A.; Paschina, G. *J. Mater. Chem.* **2002**, *12*, 1505.
(8) Casula, M. F.; Corrias, A.; Falqui, A.; Serin, V.; Gatteschi, D.; Sangregorio, C.; de Julián Fernández, C.; Battaglin, G. *Chem. Mater.* **2003**, *15*, 2201.
(9) Ennas, G.; Falqui, A.; Marras, S.; Sangregorio, C.; Marongiu, G. *Chem. Mater.* **2004**, *16*, 5659.
(10) Corrias, A.; Casula, M. F.; Ennas, G.; Marras, S.; Navarra, G.; Mountjoy, G. *J. Phys. Chem. B* **2003**, *107*, 3030.
(11) Suh, D.; Park, T. J. *Chem. Mater.* **1997**, *9*, 1903.

10.1021/cm051722y CCC: $30.25
Published on Web 11/12/2005

solution lower than 1. A clear sol was obtained after stirring for about 2 h at 80 °C, and then a final amount of water diluted in ethanol was added after cooling to room temperature. A transparent and clear alcogel was obtained after about 2 h (the $Al/H_2O/EtOH$ molar ratios were 1/1.6/63 and the Al/HNO_3 molar ratio 1/24). The procedure was slightly modified for the preparation of the Fe−Co−Al_2O_3 gels. In this case a solution of metal nitrates ($Fe(NO_3)_3 \cdot 9H_2O$, Aldrich, 98%, and $Co(NO_3)_2 \cdot 6H_2O$, Aldrich, 98%) in ethanol was added in the prehydrolysis step; as a consequence, the water needed for the partial hydrolysis of ASB arises entirely from the hydrated salts. Since the metal nitrates solution has a pH lower than 1, as the solution used in the prehydrolysis step for the Al_2O_3 sample, no nitric acid was added. Fe−Co−Al_2O_3 transparent alcogels were obtained also in this case about 2 h after adding the final portion of water diluted in ethanol. The total metal amount in the final nanocomposite was 10 wt % (Fe + Co/Fe + Co + Al_2O_3), and the Fe/Co molar ratio was 1/1.

The alcogels were aged from 2 h to 3 days and calcined at 450 °C in static air for 1 h in order to eliminate water and organics; the resulting xerogel samples were then calcined at increasing temperatures from 600 to 1200 °C; the Fe−Co−Al_2O_3 sample was reduced under H_2 flow at 800 °C for 2 h.

TG analysis and simultaneous DTA were carried out on a Mettler-Toledo TGA/SDTA 851. Thermal analysis data were collected in the 25−1000 °C range, under oxygen flow (heating rate = 10 °C·min^{-1}; flow rate = 50 mL·min^{-1}). Differential thermal analyses were carried out in the range of 25−1300 °C using a DTA Linseis model L62 in the same isochronal conditions.

XRD spectra were recorded on a X3000 Seifert diffractometer equipped with a graphite monochromator on the diffracted beam. The scans were collected within the range of 10−100° (2θ) using Cu Kα radiation.

TEM bright field (BF) and dark field (DF) images and selected-area electron diffraction (SAED) patterns were obtained on a JEOL 200CX microscope equipped with a tungsten cathode operating at 200 kV. The samples were dispersed in ethanol and dropped on a holey carbon-coated copper grid.

Textural analysis was carried out on a Sorptomatic 1990 system (Fisons Instruments), by determining the nitrogen adsorption/desorption isotherms at 77 K. Before analysis, the samples were heated to 200 °C at a rate of 1 °C·min^{-1} under vacuum. The specific surface area (S) and the pore size range were assessed by the Barrett−Emmett−Teller (BET) and the Barrett−Joyner−Halenda (BJH) methods, respectively.[12,13]

Density measurements were carried out at room temperature by heliostereopicnometry on a Quantochrome Mod SPY-2 apparatus.

Measurements of static magnetization of the sample reduced at 800 °C after thermal treatment at 450 °C was performed on a Quantum Design MPMS SQUID magnetometer, equipped with a superconducting magnet producing fields up to 50 kOe. Zero-field-cooled (ZFC) magnetization was measured by cooling samples in zero magnetic field and then by increasing the temperature in an applied field of 25 Oe, while field-cooled (FC) curves were recorded by cooling the sample in the same field. A hysteresis loop at T = 2 K was also measured on the same sample. All the magnetic data were normalized with respect to the entire mass of the sample.

Results and Discussion

As-Prepared and Calcined Al_2O_3 Xerogels. TG and DTG curves of Al_2O_3 alcogels (Figure 1) show a sharp and relevant weight loss due to solvent evaporation up to 200 °C and a slight one due to combustion of organic residues up to 600 °C. The DTA curve of a sample previouly calcined at 450 °C shows a rather sharp exothermic peak in the range centered around 1230 °C.

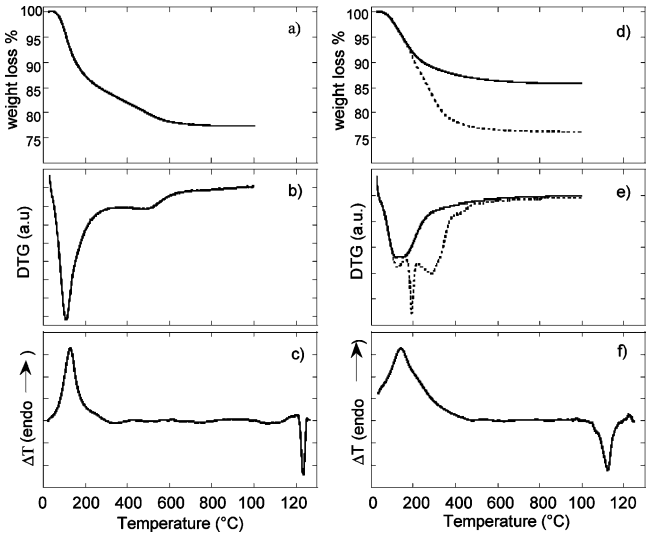

Figure 1. TG and DTG, curves of Al_2O_3 alcolgel (a−b). DTA curve of Al_2O_3 xerogel pretreated at 450 °C (c). TG and DTG curves of FeCo−Al_2O_3 samples pretreated at 150 (dashed line) and 450 °C (continuous line) respectively (d, e). DTA curve of FeCo−Al_2O_3 xerogel pretreated at 450 °C (f).

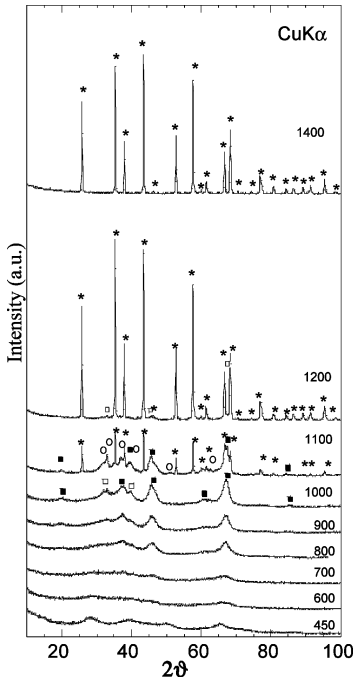

Figure 2. XRD spectra of the Al_2O_3 sample, thermally treated at different temperatures: ■, γ-Al_2O_3; ○, δ-Al_2O_3; □, ϑ-Al_2O_3; *, α-Al_2O_3.

The XRD spectra of the Al_2O_3 xerogel after thermal treatments at increasing temperatures are shown in Figure 2. The 450 °C pattern shows broad peaks corresponding to those of so-called pseudo-boehmite, $AlO(OH) \cdot nH_2O$, a hydrated form of bohemite. It is characterized by a layered structure in which AlO_6 octahedra are joined by sharing edges forming zigzagged layers, (pseudo)boehmite being actually finely- or nanosized boehmite where water molecules adsorbed on the surface lead to modification of the surface

(12) Rouquerol, F.; Rouquerol, J.; Sing, K. S. W. *Adsorption by Powders and Porous Solids: Principles, Methodology and Applications*; Academic Press: London, 1999.
(13) Brunauer, S.; Emmet, P. H.; Teller, E. *J. Am. Chem. Soc.* **1938**, *60*, 309.

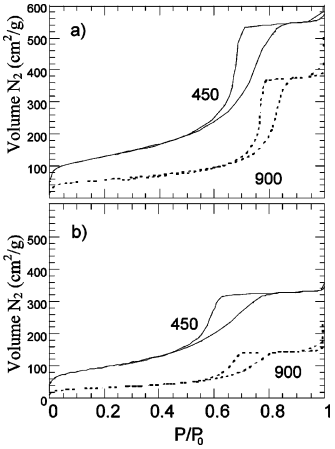

Figure 3. N_2 physisorbtion curves recorded at 77K for (a) Al_2O_3 and (b) $FeCo-Al_2O_3$ samples calcined at different temperatures.

Table 1. Surface Areas (S) and Densities (d) of the Al_2O_3 and $FeCo-Al_2O_3$ Samples Calcined at Different Temperatures[a]

	Al_2O_3		$FeCo-Al_2O_3$	
	450 °C	900 °C	450 °C	900 °C
S (m^2/g)	457	197	345	113
d (d/cm^3)	2.42(7)	3.29(8)	2.64(6)	3.67(8)

[a] Differences in surface area values obatined from repeated runs were found to be less than 5%.

layers and affect interlayer distances.[14] Calcination up to 700 °C gives rise to an increasingly disordered phase.

At 800 °C a few diffuse peaks ascribed to the formation of cubic γ-Al_2O_3 begin to appear at 2θ around 37, 46, and 67°, and they become clearly evident at 1000 °C;[15a] diffraction peaks around $2\theta = 33$ and 42° indicate the presence at this temperature of a small amount of tetragonal δ-Al_2O_3.[15b] In the XRD pattern after thermal treatment at 1100 °C main peaks are due to γ- and α-Al_2O_3;[15c] α-Al_2O_3 begins to form at this temperature, and its amount increases progressively with it. At 1200 °C XRD pattern confirms the complete γ-Al_2O_3 to α-Al_2O_3 tranformation, with some residual peaks of θ-Al_2O_3,[15d] originating from δ-Al_2O_3, which disappear after thermal treatments at 1400 °C. The observed structural evolution is in agreement with the phase transformations observed in boehmite derived gels: metastable γ-Al_2O_3 is formed first and then it evolves toward the thermodynamically stable phase, α-Al_2O_3 (corundum), through polymorphic phase transformations.[16]

The porous structure of the samples was investigated by N_2 physisorption measurements. Figure 3 shows the physisorption isotherm of the samples calcined at 450 and 900 °C, respectively. The isotherms can be classified as type IV with an H2 hysteresis loop and show a limited N_2 uptake at low relative pressure, indicating the presence of a mesoporous structure. The surface area and the density values are reported in Table 1. Surface area decreases with calcination temperatures, while density increases with it up to a value close to 85% of that of bulk γ-Al_2O_3.

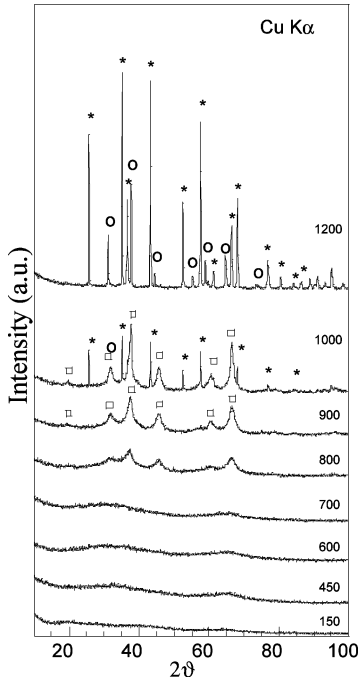

Figure 4. XRD spectra of the $FeCo-Al_2O_3$ sample, thermally treated at different temperatures: ■, γ-Al_2O_3 type; ○, $Co(Fe)Al_2O_3$ spinel; *, α-Al_2O_3.

As-Prepared and Calcined $Fe-Co-Al_2O_3$ Xerogels. TG curves of as-prepared $Fe-Co-Al_2O_3$ alcogels show a remarkable weight loss in the range of 150−400 °C due to solvent evaporation, which hide any other minor effects; solvent in these samples is present in quantities much higher than in the corresponding allumina alcogels. Analysis therefore was performed on sample portions thermally treated at 150 °C. TG and DTG curves (Figure 1 d,e) still show weight loss up to 400 °C; DTG shows a significant peak at 190 °C due to decomposition of nitrate ions and a smaller one around 350 °C due to organics combustion, both of which are shown to be exothermic by pertinent DTA (Figure 1f), where an exothermic peak centered around 1120 °C is also present.

XRD spectra of the $Fe-Co-Al_2O_3$ xerogel calcined at increasing temperatures are reported in Figure 4. Spectra in the range of 150−700 °C are typical of an amorphous phase in which metal ions are dispersed at atomic level.

Diffraction peaks which begin to appear at 800 °C are at the angular values expected for γ-Al_2O_3, although they have slightly different intensity ratios. This phase is stable up to 900 °C. Whole diffraction pattern was fitted by Rietveld refinement[17] (Figure 5a and Table 2) which reveals a phase with a structure similar to γ-Al_2O_3 where Fe(III) and Co(II) ions partially fill octahedral and tetrahedral sites, respectively. At 1000 °C α-Al_2O_3 and $Co(Fe)Al_2O_4$ begin to crystallize as evidenced by the exothermic peak in the range of 1050−1170 °C in the DTA curve, and they become the only phases present at 1200 °C. As expected, the presence of metal ions leads to phase transition temperatures lower than those of the pure matrix.

$Co(Fe)Al_2O_4$ is a cubic spinel with a γ-Al_2O_3-like structure, the tetrahedral sites being occupied by Co(II) and Fe(II)

(14) Tettenhorst, R.; Hofmann, D. A. *Clays Clay Miner.* **1980**, *28*, 373.
(15) PDF-2 File, JCPDS International Center for Diffraction Data, Swarthmore, PA: (a) no. 10-425, (b) no. 80-956, (c) no. 46-1212, (d) no. 79-1558, (e) no. 44-1433.
(16) Brinker, C. J.; Scherer, G. W. *Sol−Gel Science*; Academic Press: San Diego, 1990.
(17) Young, R. A. *The Rietveld Method*; IUCR Monographs; Oxford University Press: New York, 1995.

Table 2. Results of the Rietveld Refinements of XRD Data of FeCo−Al_2O_3 Samples[a]

	γ-Al_2O_3 type			Co(Fe)Al_2O_3			α-Al_2O_3			
sample	wt %	a_0	$\langle D\rangle$	wt %	a_0	$\langle D\rangle$	wt %	a_0/c_0	$\langle D\rangle$	R_{wp}
calcined at 900 °C	100(5)	0.7960(4)	4(1)							0.07
calcined at 1200 °C				22(1)	0.8141(1)	28(1)	78(1)	a_0 0.4771(1) c_0 1.2978(1)	55(1)	0.02

[a] Weight percentage (wt %), lattice parameters a_0 and c_0 (nm), average particle size $\langle D\rangle$ (nm), and weighted pattern agreement index R_{wp}.

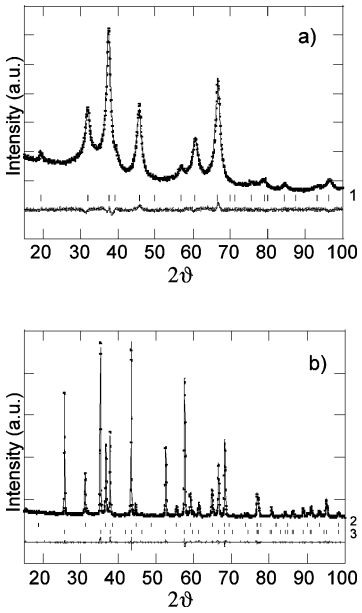

Figure 5. Experimental XRD spectra (dots), Rietveld simulation (continuous line), difference curve (bottom) of FeCo−Al_2O_3 samples treated at 900 (a) and 1200 °C (b), respectively. Vertical markers correspond to (1) γ-Al_2O_3 type, (2) Co(Fe)Al_2O_3 spinel, and (3) α-Al_2O_3.

and partially by Al(III). Residual Fe(III) and Co(II) fill octahedral sites where most of Al(III) sits. These results come from Rietveld analysis (Figure 5b and Table 2), which showed that intensity ratios of some peaks are very sensitive to the occupancy factor and to the oxidation states of metal ions. Refinement converged to a stoichiometric composition of $(Co^{2+}_{0.45}Fe^{2+}_{0.45}Al^{3+}_{0.1})[Al^{3+}_{1.80}Co^{2+}_{0.05}Fe^{3+}_{0.05}]O_4$ and to the presence of 78% Al_2O_3 and 22% spinel, which are close to the values of 82% and 18% expected by nominal composition if iron and cobalt were completely involved in the formation of such a spinel. The Fe−Co−Al_2O_3 samples are significantly different from the Fe−Co−SiO_2 ones, where calcination led to the formation of metal oxide nanoparticles dispersed in the amorphous silica matrix.[7−10] Such differences can be ascribed to the cation-deficient crystalline structure of γ-Al_2O_3 matrix that can easily accommodate metal ions by reaction with metal oxides.[16]

The evolution of the samples with calcination treatments is also accompanied by a change in color: the xerogels present a grayish color for calcination treatments up to 700 °C, while a light blue color characterizes the samples treated at higher temperatures. It should be noted that $CoAl_2O_4$ is characterized by a bright blue color, which makes it widely used as inorganic ceramic pigment.[18]

Bright field (BF) and dark field(DF) TEM images of Fe−Co−Al_2O_3 calcined at 900 °C, Figure 6, show the presence

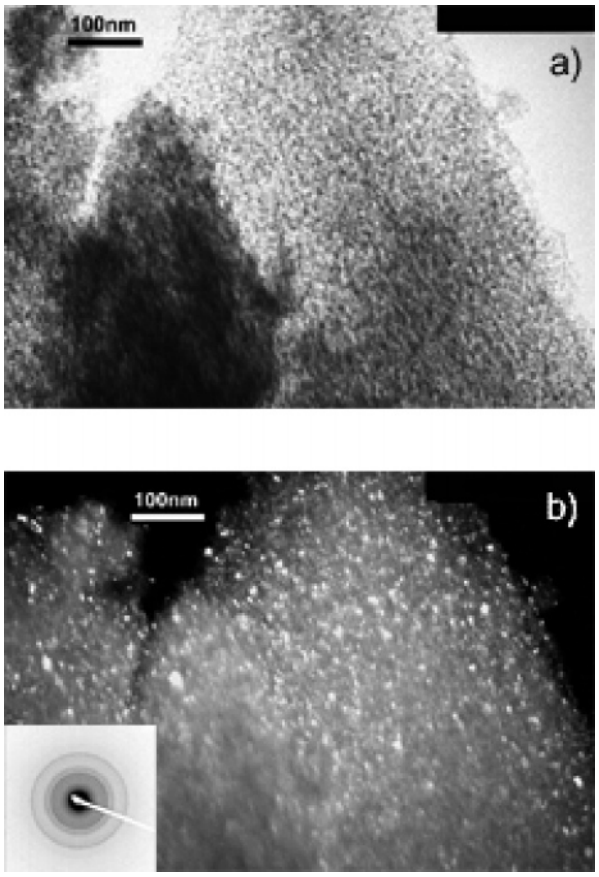

Figure 6. TEM BF (a) and corresponding DF (b) images of the FeCo−Al_2O_3 sample treated at 900 °C. Inset the electron diffraction pattern.

of round particles with a size distribution centered around 5 nm. SAED, shown in the insert, confirms XRD results on the presence of a γ-Al_2O_3 type phase.

Part b of Figure 3 reports the physisorption isotherms of the Fe−Co−Al_2O_3 samples calcined at 450 and 900 °C, respectively. The samples exhibit a type IV isotherm with an H2 hysteresis loop, indicating the same network structure of the matrix, as suggested also by the close surface area and density values reported in Table 1.

Reduced Xerogels. Reduction treatment under a hydrogen flow for 2 h at 800 °C was carried out on two xerogels previously calcined at 900 and 450 °C, respectively. XRD spectra of the reduced sample after calcination at 900 °C, shown in Figure 7a, superimposes thoroughly to that of the unreduced sample calcined at the same temperature and does not exhibit any peak ascribable to the presence of crystalline metallic phases. It is reasonable to assume that this result is the consequence of the formation at this temperature of a γ-Al_2O_3 phase, where Fe(III) and Co(II) are tightly bound in the octahedral and tetrahedral positions of the spinel structure and are not available to hydrogen reduction. On the other hand the XRD pattern of the sample reduced after

(18) Bolt, P. H.; Habraken, F. H. P. M.; Geus, J. W. *J. Solid State Chem.* **1998**, *135*, 59.

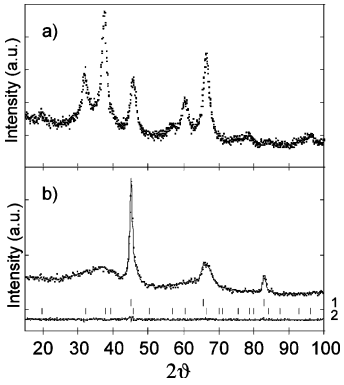

Figure 7. Experimental XRD spectra of $FeCo-Al_2O_3$ sample reduced after calcination at 900 °C (a). Experimental XRD spectra (dots), Rietveld simulation (continuous line), and difference curve (bottom) of $FeCo-Al_2O_3$ sample reduced after calcination at 450 °C (b). Vertical markers correspond to the calculated Bragg reflection of (1) CoFe alloy and (2) γ-Al_2O_3 type.

calcination at 450 °C (Figure 7b) shows a significant area and sharpness increase of the peak at $2\theta = 44.8°$, a broadening of the peak around 66°, which are both superimposed to those of γ-Al_2O_3, and the appearing of a peak at $2\theta = 82.7°$. These results are consistent with the presence of a bcc metallic nanocrystalline phase, while there is no evidence of peaks ascribable to fcc and/or hcp metallic cobalt. A qualitative inspection of the XRD pattern cannot give a definite answer to the actual formation of the bcc FeCo alloy which is difficult to distinguish from pure bcc α-Fe, the lattice parameter of the two phases being very close. Rietveld fitting, shown in the Figure 7b, leads to a cell parameter value (0.2851 nm) close to that expected for an equiatomic FeCo alloy,[15e] which is assumed to be the metallic phase present, also in agreement with the results previously reported for $FeCoSiO_2$ xerogels[9] and $FeCoAl_2O_3$ aerogels.[19] The average value of particle size obtained by Rietveld refinement is centered around 9 nm.

In Figure 8 the TEM BF and DF images of the $FeCo-Al_2O_3$ reduced samples previously calcined at 450 °C are shown. The dark spots due to FeCo alloy nanoparticles embedded in the Al_2O_3 structure are clearly visible in the BF images, the average particles size being centered around 10 nm in agreement with the XRD result. In the DF images large spots due to the FeCo alloy emerge from a background of smaller spots due to the nanocrystalline matrix. Diffraction rings of both FeCo and Al_2O_3 nanoparticles are present in the selected electron diffraction pattern shown in the insert of Figure 8b.

The ZFC and FC magnetization curves measured in the temperature range of 4.2−325 K under a static magnetic field of 25 Oe indicate a superparamagnetic behavior[20−22] of alloy nanoparticles (Figure 9a). The fact that the curves are not superimposed at $T = 325$ K points out that nanoparticles are still in the magnetic blocked state at this temperature.

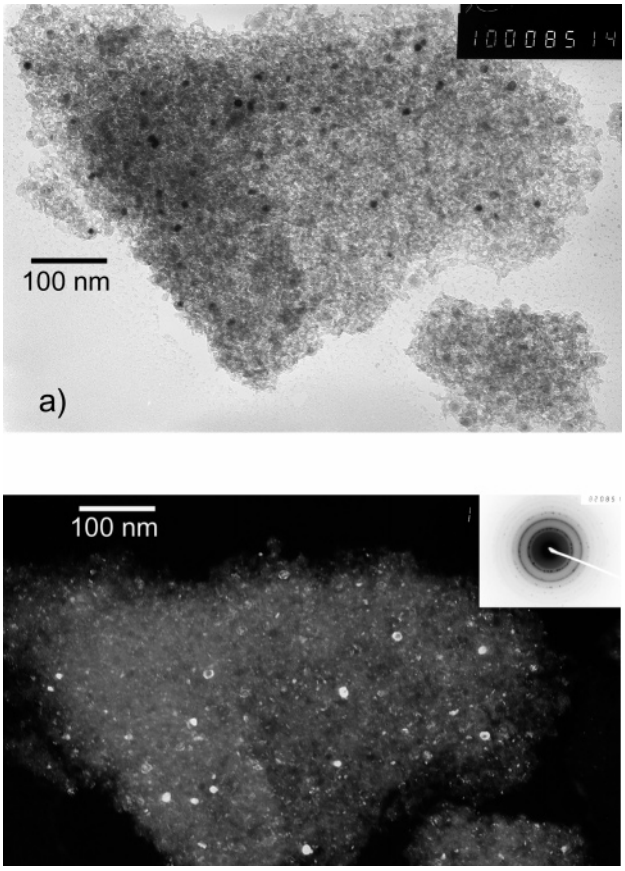

Figure 8. TEM BF (a) and corresponding DF (b) images of $FeCo-Al_2O_3$ sample reduced after calcination at 450 °C. In the insert the electron diffraction pattern is shown.

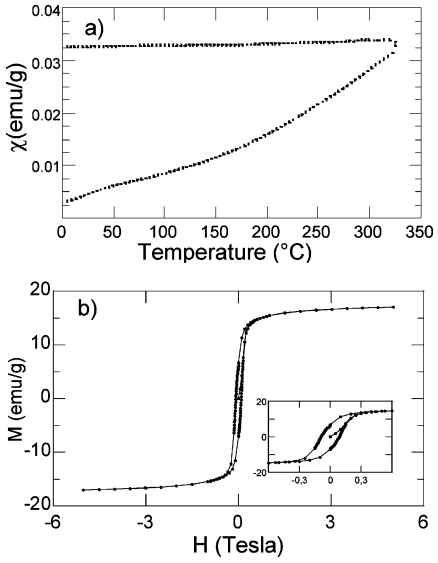

Figure 9. ZFC−FC magnetization of the $FeCo-Al_2O_3$ sample reduced after calcination at 450 °C (a) and the corresponding magnetic hysteresis loop M(H) at 2 K (b).

Considering the quite low magnetocrystalline anisotropy expected for the equiatomic FeCo alloy, it is very likely that blocking of nanoparticles is mainly due to high-strength dipolar interparticle magnetic interactions, as also suggested by the zero pendence of FC curve. This behavior can be accordingly ascribed to a transition to a magnetic collective state.[23] The strength of dipolar magnetic interactions increases

(19) Corrias, A.; Casula, M. F.; Falqui, A.; Paschina, G. *Chem. Mater.* **2004**, *16*, 3130.
(20) Morrish, A. H. *The Physical Principles of Magnetism*; Wiley: New York, 1965.
(21) Nèel, L. *Ann. Geophys.* **1949**, *5*, 99.
(22) Chantrell, R. W.; Wohlfhart E. P. *J. Magn. Magn. Mater.* **1983**, *40*, 1.

with the particle magnetic moments, proportional to particle volume and decreases with their distance. A comparison with $FeCo/Al_2O_3$ aerogel nanocomposite,[19] where nanoparticles are of comparable size, confirms this behavior. In this sample, the shape of ZFC and FC magnetization curves indicates a lower strength of particle interaction, as a consequence of larger interparticle distance due to the lower density of the aerogel matrix.

The hysteresis loop at $T = 2$ K, reported in Figure 9b, points out that the sample reaches almost complete saturation at 35 kOe, indicating that no relaxing particles are still present in the sample at this temperature for higher fields. Neglecting the slight diamagnetic contribution due to the Al_2O_3 matrix, a saturation magnetization M_s around 17.5 emu/g, extrapolated at high fields, can be inferred. Comparison with the M_s value of the bulk FeCo alloy (230 emu/g) suggests the presence of an equiatomic FeCo alloy with a weight content of 7.6%. Moreover, the reduced remanent magnetization M_r/M_s value of 0.38, well below the value expected according to Stoner and Wohlfart theory for an ensemble of not interacting superparamagnetic nanoparticles, can be further ascribed to the presence and strength of interparticle dipolar interactions.[24−25]

Conclusions

Al_2O_3 and $FeCo-Al_2O_3$ xerogels with large pore volumes and surface areas were obtained via a fast sol−gel synthesis. Calcination at increasing temperature of the $FeCo-Al_2O_3$ xerogel gives rise at 900 °C to a phase similar to γ-Al_2O_3, where Fe and Co ions partially fill the vacancies, while at 1000 °C α-Al_2O_3 and $Co(Fe)Al_2O_4$ begin to crystallize and become the only phases present at 1200 °C.

The reduction of the $FeCo-Al_2O_3$ samples previously calcined at 450 °C gives rise to the desired nanocomposites which are constituted of round FeCo alloy nanoparticles embedded into the nanocrystalline γ-Al_2O_3 matrix.

The magnetic characterization of the reduced sample indicates that it is superparamagnetic with a magnetic blocked state still at room temperature due to the presence of high-strength particle interactions.

Acknowledgment. We acknowledge Ministero dell'Istruzione, dell'Università e della Ricerca (MIUR, PRIN project) and Università di Cagliari.

CM051722Y

(23) Fiorani, D.; Dormann, J. L.; Cherkaoui, R.; Tronc, E.; Lucari, F.; D'Orazio, F.; Spinu, L.; Nogues, M.; Garcia, A.; Testa, A. M. *J. Magn. Magn. Mater.* **1999**, *196−197*, 143.
(24) Chantrell, R. W.; Walmsey, N.; Gore, J.; Maylin, M. *Phys. Rev. B* **2000**, *63*, 24410−1−14.
(25) Kechrakos, D.; Trohidou, K. N. *Phys. Rev. B* **1998**, *58*, 12169.